Molecular-Level Theoretical Model for Electrostatic Interactions within Polyelectrolyte Brushes: Applications to Charged Glycosaminoglycans

Delphine Dean,[†] Joonil Seog,[‡] Christine Ortiz,[§] and Alan J. Grodzinsky*[,†,‡]

Departments of Electrical Engineering and Computer Science, Mechanical Engineering, and Materials Science and Engineering, Massachusetts Institute of Technology, 77 Massachusetts Avenue, Cambridge, Massachusetts 02139

Received December 14, 2002. In Final Form: April 1, 2003

In this paper, we set forth a general theoretical framework to predict the nanoelectromechanical behavior of polyelectrolyte brushes and then apply it to a model system of negatively charged chondroitin sulfate glycosaminoglycan (CS-GAG) chains. We used a Poisson−Boltzmann (PB) based approach to calculate the electrostatic component of the interaction forces between polyelectrolyte molecules in a brush and to better understand how changes in polyelectrolyte fixed charge distribution affect these forces. The applicability and accuracy of three increasingly refined models were examined via a quantitative comparison with high-resolution force spectroscopy experimental data on a model CS-GAG brush system. In the first model, the polyelectrolyte brush was represented as a uniform, flat constant surface charge density. The second model approximated the polyelectrolyte brush as a uniform volume charge density. The third model represented the time-average space occupied by individual polyelectrolyte macromolecules in the brush as cylindrical rods of uniform volume charge density and finite height. This rod model approximates additional aspects of polymer molecular geometry and nonuniform molecular charge distribution inside the brush. Although the total polyelectrolyte charge was the same in all three models, both the rod and volume charge models, which accounted for the height of the brush, predicted much higher forces than the surface charge model at any given separation distance. The comparison between measured and theoretically predicted forces showed that the rod model gave better agreement with the force data over the widest range of separation distance D and for reasonable best-fit values of the brush height and rod radius. Therefore, in the framework of the PB theory, it appears that molecular-level changes in the charge distribution inside polyelectrolyte brush layers as manifested in the rod model can significantly change the magnitude and the shape of the resulting force profile.

Introduction

Polyelectrolyte brush systems are important in many areas of polymer physics, surfactant science, biophysics, cell biology, and physiology and have technological applications in colloid stabilization, surface lubrication, stimulus-responsive surfaces, and optoelectronics. Tethered polyelectrolyte brushes also occur as natural components of biological tissues and on cell surfaces and play a significant role in their mechanical, chemical, and hydrodynamic properties.[1,2] In this paper, we set forth a general theoretical framework to predict the nanoelectromechanical behavior of polyelectrolyte brushes and then apply it to a model system consisting of negatively charged biological macromolecules known as chondroitin sulfate glycosaminoglycans (CS-GAGs).[3,4] CS-GAGs have been studied extensively, as their intermolecular electrostatic repulsive forces are responsible for >50% of the equilibrium compressive modulus of the articular cartilage.[3] CS-GAGs have a contour length of ∼35 nm, and in cartilaginous tissues most CS-GAGs are covalently bound 2−4 nm apart along a core protein to form the brushlike proteoglycan, aggrecan.[5] We have recently reported direct molecular-level measurements of the repulsive interactions of an end-grafted CS-GAG brush layer using the technique of high-resolution force spectroscopy (HRFS) in aqueous solution.[6] The CS-GAG model system provides a wide variety of experimental conditions with which to rigorously test theoretical predictions, including ionic strength, pH, and grafting density.

There have been several different approaches used in the literature for modeling polyelectrolyte brush interactions. Molecular dynamic simulations of individual polyelectrolyte macromolecules have provided information on chain conformation and supramolecular structure. However, since brush layers involve the interactions between many molecules (e.g., polymer chains, ions, and water molecules), this technique is computationally intensive and currently has limited application for predicting brush interaction forces at physiological conditions.[7] Scaling theory is another method used to characterize polyelectrolyte brush interactions[8−10] and provides straightforward analytical solutions.[8] However, each scaling law can

* Corresponding author. Department of Electrical Engineering and Computer Science, RM 38-377, 77 Massachusetts Avenue, Cambridge, MA 02139.
[†] Department of Electrical Engineering and Computer Science.
[‡] Department of Mechanical Engineering.
[§] Department of Materials Science and Engineering.

(1) Alberts, B.; Bray, D.; Lewis, J.; Raff, M.; Roberts, K.; Watson, J. D. *Molecular Biology of the Cell*; Garland: New York, 1994.
(2) de Kruif, C. G.; Zhulina, E. B. *Colloids Surf., A* **1996**, *117*, 151.
(3) Buschmann, M. D.; Grodzinsky, A. J. *J. Biomech. Eng.* **1995**, *117*, 179−192.
(4) Ehrlich, S.; Wolff, N.; Schneiderman, R.; Maroudas, A.; Parker, K. H.; Winlove, C. P. *Biorheology* **1998**, *35*, 383−397.
(5) Muir, I. H. M. In *Adult Articular Cartilage*; Freeman, M. A. R., Ed.; Pitman Medical: Kent, U.K. 1979; pp 215−290.
(6) Seog, J.; Dean, D.; Plaas, A. H. K.; Wong-Palms, S.; Grodzinsky, A. J.; Ortiz, C. *Macromolecules* **2002**, *35*, 5601−5615.
(7) Csajka, F. S.; Seidel, C. *Macromolecules* **2000**, *33*, 2728−2739.
(8) Pincus, P. *Macromolecules* **1991**, *24*, 2912−2919.
(9) Rabin, Y.; Alexander, S. *Europhys. Lett.* **1990**, *13*, 49−54.

10.1021/la027001k CCC: $25.00
Published on Web 05/29/2003

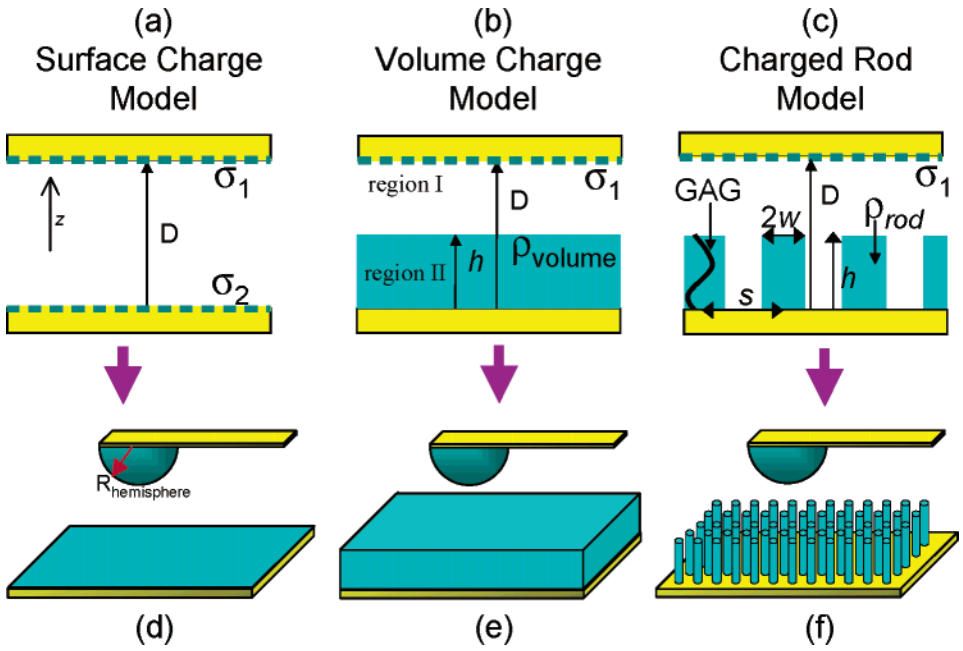

Figure 1. Schematic of (a) constant surface charge model, (b) constant volume charge model, and (c) charged rod model in plane parallel geometry. (d−f) Schematic of the models with tip approximated as a hemisphere that were used when comparing to experimental HRFS data.

only be applied to certain distinct sets of experimental conditions (e.g., solution ionic strength, pH, polymer density, chain length).[10] Continuum theory, for example, Poisson−Boltzmann (PB) based models,[11−13] is applicable to a wide range of experimental conditions while still remaining computationally tractable and allows direct quantitative comparison with experimental data. However, the PB approach does not account for structure and interactions at the atomic level.

The objective of this study was to use a continuum approach to model the electrostatic component of interactions between polyelectrolyte molecules in a brush layer, to calculate the nanoscale electrostatic interaction forces, and to better understand how molecular-level changes in the fixed charge distribution affect these interaction forces. The applicability and accuracy of three increasingly refined theoretical models (Figure 1) based on the PB equation were examined via a rigorous quantitative comparison with HRFS experimental data on a model CS-GAG brush system.[6] The PB approach predicts the electrostatic double-layer force between charged surfaces due to electrical and osmotic interactions associated with polyelectrolyte fixed charge and the mobile ions in solution. The first two models have been reported previously in the literature,[12,14] and the third newly developed model is reported here for the first time. Each of the three models employs increasingly more geometrically specific representations of the polyelectrolyte macromolecular fixed charge.

In the first model (Figure 1a), a polyelectrolyte brush layer is represented as a uniform, flat constant surface charge density.[14] The second model (Figure 1b) approximates the polyelectrolyte brush as a uniform volume charge density.[12] Even though this model takes into account the height of the brush, the molecular shape and charge distribution along the polyelectrolyte chain backbone are not included. The third model (Figure 1c) represents the time-average space occupied by the individual polyelectrolyte macromolecules in the brush as cylindrical rods of uniform volume charge density and finite height. This approach attempts to account for additional aspects of polymer molecular geometry and nonuniform molecular charge distribution inside the brush. This model is different from the "unit cell" model[15] where each polyelectrolyte macromolecule is represented as an infinitely long cylinder having a fixed surface charge.

First, the electrical potential and the spatial distribution of ions were computed in the region between a planar brush layer and a charged planar surface situated above the brush as a function of separation distance *D*, shown in Figure 1a−c. Then, the electrostatic forces between the brush and the charged planar surface predicted by each of these three models were compared to each other using a range of model parameters and bath ionic strengths. The models were then adapted to the experimental configuration[6] of Figure 2, incorporating the geometry of a hemispherical probe tip with known surface charge density situated above the brush (Figure 1d−f) instead of the charged planar surface.[16] Model predictions were then compared to HRFS measurements of the total repulsive force reported in the literature by us.[6] Because the equations relating the electrostatic force to the known system parameters (e.g., GAG charge density and bath ionic strength) are nonlinear and are difficult to solve analytically, finite difference methods (FDM) were used to obtain numerical solutions of the models.

General Theoretical Methods

The PB equation relates the spatial distribution of the electrical potential, Φ, in an electrolyte solution[17,18] to the

(10) von Goeler, F.; Muthukumar, M. *J. Chem. Phys.* **1996**, *105*, 11335−11346.
(11) Fixman, M. *J. Chem. Phys.* **1979**, *70*, 4995−5005.
(12) Ohshima, H. *Colloid Polym. Sci.* **1999**, *277*, 535−540.
(13) Tamashiro, M. N.; Hernández-Zapata, E.; Schorr, P. A.; Balastre, M.; Tirrell, M.; Pincus, P. *J. Chem. Phys.* **2001**, *115*, 1960−1969.
(14) Butt, H.-J. *Biophys. J.* **1991**, *60*, 777−785.
(15) Katchalsky, A. *Pure Appl. Chem.* **1971**, *26*, 327−373.
(16) Bhattacharjee, S.; Elimelech, M. *J. Colloid Interface Sci.* **1997**, *193*, 273−285.
(17) Devereux, O. F.; de Bruyn, P. L. *Interaction of plane-parallel double layers*; M.I.T. Press: Cambridge, MA, 1963.
(18) Verwey, E. J. W.; Overbeek, J. T. G. *Theory of the Stability of Lyophobic Colloids*; Elsevier: Amsterdam, 1948.

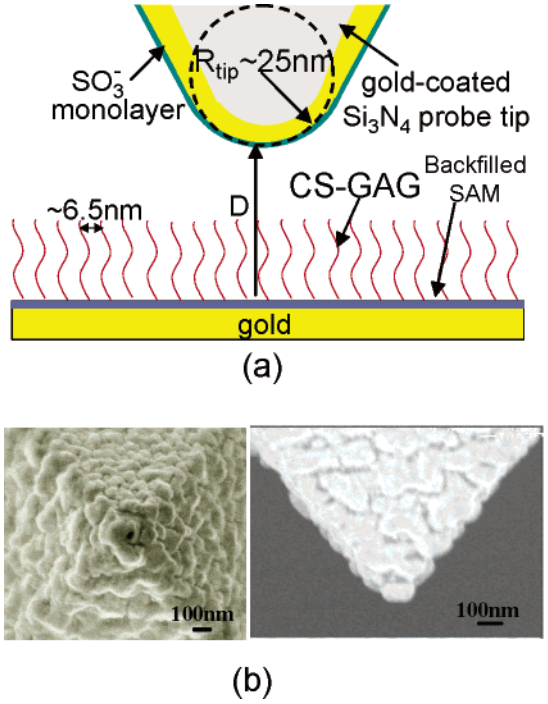

Figure 2. (a) Schematic of high-resolution force spectroscopy configuration using a Au-coated sulfate-functionalized probe tip above an end-grafted CS-GAG polymer brush. (b) Bottom and side view scanning electron photomicrographs of the probe tip.

concentration of fixed and mobile charges within the electrolyte and at the boundaries of the solution phase, that is, the charges that are the source of the electric field and potential. The resulting Φ obtained from solution of the PB equation can then be used to compute forces of electrical origin on charged species or structures (e.g., a hemispherical probe tip) within the region of interest. The PB equation is based on several simplifying assumptions[18,19] including the following: (a) the permittivity, ϵ, is everywhere the same as that of the bulk solution, ϵ_w ($=6.92 \times 10^{-10}$ C/N·m^2), and is independent of the electric field, (b) time-varying magnetic fields are negligible (i.e., the system is electroquasistatic), (c) the ions in solution are treated as point charges and therefore take up no volume, and (d) the system is assumed to be in thermodynamic equilibrium.

From assumption a above, the electric field, **E**, can be related to the total volume space charge density, ρ_{total}, using Gauss's law:

$$\nabla \cdot \epsilon \mathbf{E} = \epsilon_w \nabla \cdot \mathbf{E} = \rho_{total} \tag{1}$$

In general, **E** is related to the time-varying magnetic field, **H**, using Faraday's law:

$$\nabla \times \mathbf{E} = -\frac{\partial}{\partial t}(\mu \mathbf{H}) \approx 0 \tag{2}$$

When the time rates of change in eq 2 are small enough or the magnetic field is negligibly small, the right-hand side (RHS) of eq 2 tends to zero (assumption b above) and we can then define a scalar electrical potential, Φ, related to the quasistatic **E** field by

$$\mathbf{E} = -\nabla \Phi \tag{3}$$

which automatically satisfies the quasistatic form of eq 2. From eqs 1 and 3, the potential and space charge distribution are then related by Poisson's equation:

$$\nabla^2 \Phi = -\frac{\rho_{total}}{\epsilon_w} \tag{4}$$

In our system, the total space charge, ρ_{total}, is the sum of that due to the mobile ions in solution, ρ_{mobile}, and any fixed charges present, ρ_{fix}:

$$\nabla^2 \Phi = -\left(\frac{\rho_{mobile} + \rho_{fix}}{\epsilon_w}\right) \tag{5}$$

The ion distributions in solution are assumed to obey Boltzmann statistics in thermodynamic equilibrium, and therefore, the ith mobile ion concentration c_i is related to the potential by

$$c_i = c_{io} \exp\left(-\frac{z_i F}{RT}\Phi\right) \tag{6}$$

where z_i is the valence of species i, F is the Faraday constant (=96 500 C/mol), R is the universal gas constant (=8.314 J/mol·K), T is the absolute temperature (=298 K), and the reference potential $\Phi = 0$ is taken to be the potential of the bath where $c_i = c_{io}$. In eq 6, the potential of the average force on the ions is assumed to be the electrical potential of the mean field in Poisson's eq 4.[11] From eq 6, the total charge density can be expressed as

$$\rho_{total} = \sum_i z_i F c_{io} \exp\left(-\frac{z_i F \Phi}{RT}\right) + \rho_{fix} \tag{7}$$

Poisson's eq 5 then takes the general form of the Poisson–Boltzmann equation:

$$\nabla^2 \Phi = -\frac{\left(\sum_i z_i F c_{io} \exp\left(-\frac{z_i F \Phi}{RT}\right) + \rho_{fix}\right)}{\epsilon_w} \tag{8}$$

For an electrolyte bath containing a monovalent salt (such as NaCl) having bath concentration C_0, and assuming that C_0 is significantly greater than the concentration of ions coming from the dissociation of fixed charge groups (e.g., the concentration of protons coming from dissociation of GAG carboxylate and sulfate fixed charge groups is small compared to bath NaCl), then eq 8 reduces to the familiar 1:1 electrolyte form of the Poisson–Boltzmann equation[17,20] with an added fixed charge term:

$$\nabla^2 \Phi = \frac{2FC_0}{\epsilon_w} \sinh\left(\frac{F\Phi}{RT}\right) - \frac{\rho_{fix}}{\epsilon_w} \tag{9}$$

To uniquely determine the potential from eqs 8 or 9, two boundary conditions on either the potential or its derivative (the electric field) are required. In this study, constant charge boundary conditions on both bounding surfaces are employed because in the experiments,[6] neither the probe tip nor the substrate is electrically connected to any source that would maintain them at a

(19) Honig, B.; Nicholls, A. *Science* **1995**, *268*, 1144–1149.

(20) Sanfeld, A. *Thermodynamics of charged and polarized layers*; Wiley-Interscience: Bath, U.K., 1968; Vol. 10.

constant potential.[21] In addition, the surface charge of the tip and the GAG charge on the substrate are initially known, and they are essentially constant within the range of bath pH and ionic strength conditions used (see Appendix A). For example, if the charge on the tip is defined as σ_1 and the charge on the substrate surface as σ_2 in Figure 1a, then from Gauss's law with the *z*-direction defined as shown in Figure 1a, the boundary conditions at those surfaces will be $\partial\Phi/\partial z = \sigma_1/\epsilon_w$ and $\partial\Phi/\partial z = -\sigma_2/\epsilon_w$, respectively. The length scale over which the electrostatic potential decays is known as the Debye length, κ^{-1}, which comes from the solution of the linearized Poisson Boltzmann eq 8 and takes the following form with valence $z_i = 1$:

$$\kappa^{-1} = \sqrt{\frac{\epsilon_w RT}{2F^2 C_0}} \tag{10}$$

From eq 6, the counterion and co-ion concentrations in the fluid phase in thermodynamic equilibrium are related to the potential as

$$c_+ = C_0 \exp\left(-\frac{F}{RT}\Phi\right) \tag{11}$$

$$c_- = C_0 \exp\left(+\frac{F}{RT}\Phi\right)$$

Once the potential, Φ, has been determined from solution of the PB equation, the electrostatic free energy can be calculated from the spatial distribution of the potential:[22,23]

$$W_e(z,q) = \int_{\text{surface}} \sigma\Phi \, dS + \int_{\text{volume}} \rho_{\text{fix}}\Phi \, dV - \int_{\text{volume}} \left(2RTC_0\left(\cosh\left(\frac{F\Phi}{RT}\right) - 1\right) + \frac{\epsilon_w}{2}(\nabla\Phi)^2\right) dV \tag{12}$$

where *q* is charge. The total electrostatic free energy in eq 12 is the sum of terms associated with (a) fixed charge groups on surfaces or in the volume (i.e., the first and second terms on the RHS) and (b) mobile ionic charges (e.g., Na^+, Cl^-) in solution, which give rise to local osmotic and electric field stresses (i.e., the third and fourth terms on the RHS of (12), respectively).[22]

Finally, the *z*-component of the force of electrical origin acting in the *z*-direction on the upper surface of the system of Figure 1 can be calculated from the *z*-derivative of the free energy while keeping the charge constant:

$$F_z = \left(-\frac{\partial}{\partial z}(W_e)\right)\Big|_{q \text{ constant}} \tag{13}$$

This force is equal and opposite to that acting on the lower surface containing the brush layer. The PB equation is generally nonlinear and is therefore difficult to solve analytically except for cases in which the boundary conditions have a simple geometric structure. Therefore, numerical techniques are used to solve the models below.

Models of Electrostatic Free Energy and Force

Constant Surface Charge Model.[14,24] The first model (Figure 1a) has been used in the literature[25−27] to approximate the electrostatic force caused by deformation of a polyelectrolyte brush. All fixed charges on the polyelectrolytes are represented as a constant charge density that is collapsed on a surface, and there is no bulk fixed charge density away from the surface ($\rho_{\text{fix}} = 0$). In this case, the Poisson−Boltzmann eq 9 reduces to

$$\nabla^2\Phi = \frac{2FC_0}{\epsilon_w}\sinh\left(\frac{F\Phi}{RT}\right) \tag{14}$$

When the separation distance, *D*, between the two charged planes is large compared to the Debye length ($\kappa D \gg 1$), an analytical solution[28,29] for the potential can be obtained from the nonlinear PB equation. However, as the two charged planes are brought closer together, this analytical solution is no longer valid and to obtain the force as a function of surface separation distance a Newton−Raphson method on finite differences[30,31] was used to solve the nonlinear PB equation subject to one boundary condition at each surface. The force between two charged planes of infinite extent (Figure 1a) was first obtained. Then, to compare to the experimental HRFS data, this force per unit area was numerically integrated to give the total force between a hemispherical tip and planar substrate of infinite extent (Figure 1d). Since this problem is one-dimensional, the potential in space can be represented as a one-dimensional matrix or vector in which each entry is the potential at *N* evenly spaced points along the *z*-direction. The derivatives in the *z*-direction can be calculated as differences between neighboring points. The PB equation for each discrete entry plus the boundary conditions give a set of *N* nonlinear equations all satisfied if the potential at each point is correct. If a close enough initial guess for the value of the potential at all points is given, then that guess can be refined using a Taylor series expansion. This is repeated iteratively until the change in potential at each step is smaller than an error threshold. This algorithm is known as a Newton−Raphson method for solving multidimensional systems.[31] The geometry at the end of the blunted square pyramidal probe tip (Figure 2b) was modeled as a hemisphere whose radius, $R_{\text{hemisphere}}$, is equal to the radius of curvature of the probe tip, R_{tip} (Figure 1d). This hemispherical geometry is approximated by using the calculated force between the flat surfaces and summing up the force on appropriately sized concentric cylinders. This method, based on the original formulation of Derjaguin[32] and sometimes known as surface element integration,[16] is the numerical version of the integral of a uniform normal stress or pressure over the surface of the hemisphere tip (see Appendix B). When comparing model predictions to experimental data, no fitting parameters were employed since the charge density due to the sulfate monolayer on the tip, $\sigma_{\text{tip}} = \sigma_1$, and the

(21) The Asylum MFP design is such that certain types of highly conducting tips can be grounded via the spring clip that holds the cantilever chip; however, this was not the case for our system: Cleveland, J. Asylum Research, personal communication.

(22) Sharp, K. A.; Honig, B. *J. Phys. Chem.* **1990**, *94*, 7684−7692.
(23) Shestakov, A. I.; Milovich, J. L.; Noy, A. *J. Colloid Interface Sci.* **2002**, *247*, 62−79.
(24) Parsegian, V. A.; Gingell, D. *Biophys. J.* **1972**, *12*, 1192−1204.
(25) Abraham, T.; Giasson, S.; Gohy, J. F.; Jerome, R. *Langmuir* **2000**, *16*, 4286−4292.
(26) Abe, T.; Higashi, N.; Niwa, M.; Kurihara, K. *Langmuir* **1999**, *15*, 7725−7731.
(27) Zauscher, S.; Klingenberg, D. J. *J. Colloid Interface Sci.* **2000**, *229*, 497−510.
(28) Gouy, G. *J. Phys.* **1910**, *9*, 457−468.
(29) Chapman, D. L. *Philos. Mag.* **1913**, *25*, 475−481.
(30) Forsythe, G. E.; Wasow, W. R. *Finite Difference Methods for Partial Differential Equations*; John Wiley & Sons: New York, 1960.
(31) Rao, S. S. In *Applied numerical methods for engineers and scientists*; Prentice Hall: Upper Saddle River, NJ, 2002; pp xx, 1060.
(32) Derjaguin, B. V. *Kolloid Z.* **1934**, *69*, 155−164.

Table 1. Model Parameters Used to Compare the Surface, Volume, and Rod Model Predictions to HRFS Experimental Data[a]

parameters	surface model	volume model	rod model
σ_1 (C/m^2) (ref 6)	-0.015	-0.015	-0.015
Q (C) (ref 6)	-8.00×10^{-18}	-8.00×10^{-18}	-8.00×10^{-18}
s (nm) (ref 6)	6.5	6.5	6.5
h (nm)	NA	variable	variable
w (nm)	NA	NA	variable
$\sigma_2 = Q/s^2$ (C/m^2)	-0.19	NA	NA
$\rho_{volume} = Q/(s^2h)$ (C/m^3)	NA	$-0.19/h$	NA
$\rho_{rod} = Q/(\pi w^2 h)$ (C/m^3)	NA	NA	$-8.00 \times 10^{-18}/(\pi w^2 h)$

[a] The parameters denoted as variable (h and w) were adjusted to fit the data using the method of least squares.

effective charge density due to the GAG brush on the substrate, $\sigma_{GAG} = \sigma_2$, are both known (see Table 1).

Volume Charge Model. The length of polyelectrolyte macromolecules in a brush layer is often much longer than κ^{-1}; for example, in the model system of interest the GAG contour length is ~35 nm and $\kappa^{-1} \sim 1$ nm at physiological ionic strength (IS). Under these conditions, the brush can be modeled as a region of uniform fixed volume charge density, ρ_{volume}, using the approach of Ohshima[12] (Figure 1b). As with the planar surface charge model, the force is first calculated numerically using infinite plate geometry (Figure 1b) and then, to compare to experimental data, converted to a hemispherical geometry (Figure 1e).

In the electrolyte region I above the fixed volume charge (Figure 1b), the PB equation has the form of eq 14. In region II inside the fixed volume charge, the PB equation has a term accounting for the polyelectrolyte brush fixed volume density, ρ_{volume}:

$$\nabla^2\Phi = \frac{2FC_0}{\epsilon_w}\sinh\left(\frac{F\Phi}{RT}\right) - \frac{\rho_{volume}}{\epsilon_w} \qquad (15)$$

Since this is a two-region problem, the solutions to eq 14 in region I and eq 15 in region II are subject to boundary conditions at the tip and substrate surfaces and at the interface between the volume charge and the electrolyte bath (Figure 1b). At the surfaces, the boundary conditions from Gauss's law have the same form as before: at the tip, the derivative of the potential is proportional to the tip surface charge density ($\partial\Phi/\partial z = \sigma_1/\epsilon_w$); at the substrate surface, however, there is no longer a surface monolayer of charge and, therefore, $\partial\Phi/\partial z = -\sigma_2/\epsilon_w = 0$. In practice, there may be some induced surface charge on the substrate but that charge can be shown to be negligible compared to the volume charge density associated with the polyelectrolyte brush. At the interface between the polyelectrolyte volume charge density and the electrolyte bath, the potential and its derivative (the electric field) must be continuous. Having obtained solutions for the potential from eqs 14 and 15, the electrostatic free energy can now be computed as before. The fixed volume charge term in the free energy calculation of eq 12 is now specified as that associated with the brush volume:[22]

$$W_e = \int_{tip}\sigma_1\Phi\, dS + \int_{brush}\rho_{volume}\Phi\, dV_b - \int_{volume}\left(2RTC_0\left(\cosh\left(\frac{F\Phi}{RT}\right) - 1\right) + \frac{\epsilon_w}{2}(\nabla\Phi)^2\right) dV \qquad (16)$$

When the distance between the surfaces, D, is less than the initial height of the volume charge, h (i.e., the initial brush height), the model reduces to that of a single region containing a volume fixed charge density. The PB equation in this case has the form

$$\nabla^2\Phi = \frac{2FC_0}{\epsilon_w}\sinh\left(\frac{F\Phi}{RT}\right) - \frac{\rho'_{volume}}{\epsilon_w} \qquad (17)$$

where $\rho'_{volume} = (\rho_{volume}h)/D$. While the PB equation is nonlinear, the problem is still one-dimensional due to symmetry and thus can be solved numerically using a method similar to that described for the surface model above. To compare this model to the data, there is one fitting parameter, h, since the brush height of the GAG on the substrate may differ from the GAG contour length and is therefore unknown. The volume charge density in the brush, ρ_{volume}, depends on the brush height, $\sigma_{GAG}/h = -0.19/h$ C/m^3, and the other parameters are fixed to their known values (Table 1).

Charged Rod Model. When polyelectrolyte macromolecules in a brush (Figure 1c) are separated by lateral distances, s, greater than κ^{-1}, there is a nonuniform distribution of charge inside the brush layer which will affect the force in a manner not predicted by the smooth uniform volume or surface charge models described above. For example, in our experiment,[6] the end-grafted GAG polyelectrolyte macromolecules are ~6.5 nm apart while $\kappa^{-1} \sim 1$ nm at physiological IS. We have therefore developed a more refined "charged rod" model in which a rod-shaped circular cylinder having radius w, finite height h, and fixed uniform volume charge density ρ_{rod} represents the time-averaged space occupied by an individual polyelectrolyte chain and its fixed charge groups (Figure 1c). The charged rods are separated by regions of zero fixed charge. When $w \geq (s^2/\pi)^{1/2}$, the charged rod model becomes equivalent to the volume charge model described above. Upon conversion of the planar geometry, the probe tip is represented as a hemisphere with constant surface charge density, σ_1, and the planar substrate−polyelectrolyte brush becomes a field of rods, each with volume charge density ρ_{rod} (Figure 1f).

In the fluid region between or above the rods, the PB equation has the form of eq 14. Inside the rods, the PB equation has an additional term accounting for the fixed volume charge density, ρ_{rod}:

$$\nabla^2\Phi = \frac{2FC_0}{\epsilon_w}\sinh\left(\frac{F\Phi}{RT}\right) - \frac{\rho_{rod}}{\epsilon_w} \qquad (18)$$

The free energy calculation is also modified slightly from the volume charge model equation:

$$W_e = \int_{tip}\sigma_1\Phi\, dS + \sum_{rods}\left(\int_{rod}\rho_{rod}\Phi\, dV_r\right) - \int_{volume}\left(2RTC_0\left(\cosh\left(\frac{F\Phi}{RT}\right) - 1\right) + \frac{\epsilon_w}{2}(\nabla\Phi)^2\right) dV \qquad (19)$$

The configuration of Figure 1c,f is also a two-region problem, and boundary conditions are applied at the tip

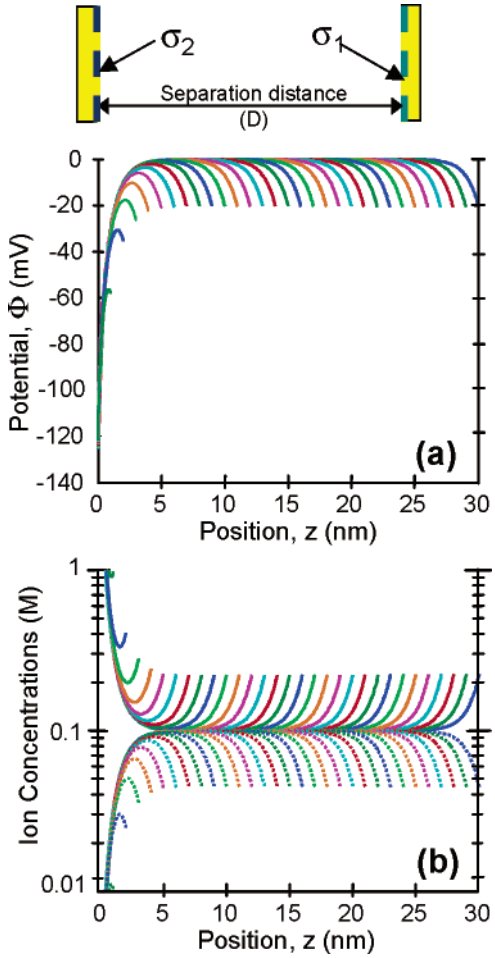

Figure 3. Spatial profiles of (a) electrical potential, Φ (mV), and (b) counterion (solid lines) and co-ion (dotted lines) concentrations (M) for the surface charge model (Figure 1a) as a function of position, z (nm). Profiles are plotted at 1 nm increments of D with $\sigma_1 = -0.015$ C/m^2, $\sigma_2 = -0.19$ C/m^2, and $C_0 = 0.1$ M.

and substrate surfaces and at the peripheral edge surrounding each rod (Figure 1c). At the tip and substrate surfaces, the boundary conditions are the same as in the volume model above. Along the interface between the rod-shaped volume charge density and the electrolyte phase, the potential and the electric field must be continuous. When $D < h$, the rod height is set to be D and the radius of the rod is expanded to keep the total rod volume and therefore ρ_{rod} constant. When $w = (s^2/\pi)^{1/2}$, the rod model is equivalent to the volume charge model of Figure 1b, and ρ_{rod} is scaled appropriately with D.

To solve for the potential in space, the rod model was first subdivided into a single rectangular repeat unit containing one rod (repeat unit size: $s \times s \times D$, see Figure 6). Since this unit has no further symmetry, the potential everywhere in space surrounding and within the single repeat unit was solved numerically using the Newton−Raphson method with an inequivalent Jacobian on a 3D finite difference grid.[31] To compare this model to the HRFS experimental data, there were two fitting parameters, h and w, since both the brush height and the space occupied by one polyelectrolyte chain on the substrate are unknown. The volume charge density in the brush, ρ_{rod}, was $(-8.0 \times 10^{-18}/(\pi h w^2))$ C/m^3 (i.e., the known fixed charge per GAG chain divided by the known volume it occupies[6]), and the other parameters (s, σ_1, and C_0) were fixed to their known values (Table 1).

Experimental Measurements

The force between a chemically end-grafted CS-GAG brush layer and a sulfate-functionalized probe tip (negatively charged at the solution C_0 and pH used, p$K_a = 2$) was measured in the configuration of Figure 2 using a cantilever-based instrument, the molecular force probe[6] (MFP, Asylum Research, Santa Barbara, CA). CS-GAG molecules were prepared from aggrecan proteoglycans that were synthesized by rat chondrosarcoma cells and metabolically radiolabeled in culture [see Seog et al.[6] for details]. The GAG contour length was calculated to be 35 nm, which includes a 3 nm linkage region containing carbohydrate and amino acid moieties. The CS-GAG chains were end-grafted onto 1 cm × 1 cm gold-coated silicon substrates using methods previously described.[6] The GAG grafting density on the wafer was calculated to be ~(6.5 nm × 6.5 nm) area per chain. Based on the known charge distribution along CS-GAG chains, this grafting density corresponds to a brush layer volume fixed charge density of $\rho_{volume} \approx -10^7$ C/m^3 (Table 1) or, equivalently, a molar fixed charge density of $|(\rho_{volume}/F)| \approx 0.1$ M. Repulsive forces between the CS-GAG chains and a chemically modified gold-coated Si_3N_4 tip ($R_{tip} = 25$ nm) functionalized with a sulfate monolayer[6] ($\sigma_1 = -0.015$ C/m^2) were then measured in NaCl solutions in the concentration range of $C_0 = 0.01-1.0$ M at pH 5.6. Thus, C_0 was varied over the range of 0.1−10 times the molar volume fixed charge density of the brush layer (ρ_{volume}/F).

Results and Discussion

Model Predictions of Electrical Potential and Ion Concentration Profiles. We first compare and contrast the three model predictions of the electrical potential, Φ, and ion concentration profiles, c_- and c_+, in the planar configurations as a function of the intersurface separation distance, D, the position within the intersurface gap, z, the bulk NaCl salt concentration (C_0), the volume charge height, h, and charged rod width, w (Figures 3−6). These results will aid in the visualization of the spatial distribution of counterions and co-ion, the subsequent comparison of electrostatic interaction forces predicted by the models, and the comparison of model predictions with experimental data.

Constant Surface Charge Model. $\Phi(z)$ predicted by the surface charge model for two planar charged surfaces is shown in Figure 3a for 1 nm increments of D and a physiologically relevant $C_0 = 0.1$ M ($\kappa^{-1} = 1$ nm). The values of the surface charge densities determined by previous experiments (σ_1 and σ_2, Table 1) are assumed to remain constant as D varies (constant charge boundary conditions, Appendix A). It is first important to note that the reference zero potential is that in the bath solution in all three models. When the surfaces are far apart compared to $\kappa^{-1} = 1$ nm (i.e., $\kappa D > 5$, or $D > 5$ nm in Figure 3a), there is minimal interaction between the two surfaces, and the potential profile has a maximum value very close to zero. Therefore, the counterion (Na^+) and co-ion (Cl^-) concentrations between the two surfaces (Figure 3b) are equal to C_0 when $\kappa D > 5$ at positions, z, a few κ^{-1} away from either surface. When $\kappa D < 5$, the potentials at each surface begin to interact strongly, and the maximum potential between the surfaces is less than zero; therefore, the counterion concentration becomes higher and the co-ion concentration lower than C_0.

Volume Charge Model. $\Phi(z)$, predicted by the volume charge model, is shown in Figure 4a for 1 nm increments of D, $C_0 = 0.1$ M ($\kappa^{-1} = 1$ nm), using values for the volume and surface charge density and brush height relevant to our previous HRFS GAG experiments (Table 1, $\sigma_1 = -0.015$ C/m^2, $\rho_{volume} = -9.44 \times 10^6$ C/m^3, $h = 20$ nm). When the surfaces are far apart (i.e., $D > 25$ nm), the potential is uniform throughout most of the brush region and is negative compared to the zero reference potential

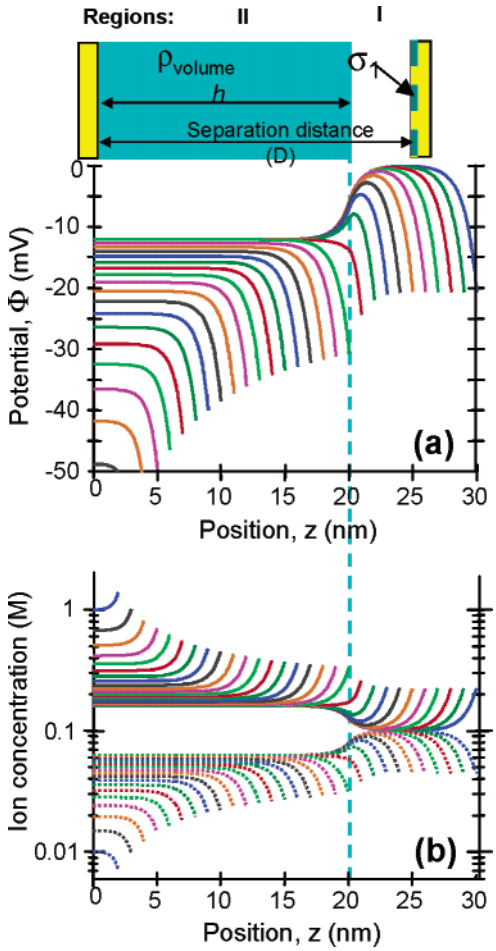

Figure 4. Spatial profiles of (a) electrical potential, Φ (mV), and (b) counterion (solid lines) and co-ion (dotted lines) concentrations (M) for the volume charge model (Figure 1b) as a function of position, z (nm). Profiles are plotted at 1 nm increments of D, with $h = 20$ nm, $\rho_{volume} = -9.44 \times 10^6$ C/m^3 (0.0978 M), $\sigma_1 = -0.015$ C/m^2, and $C_0 = 0.1$ M.

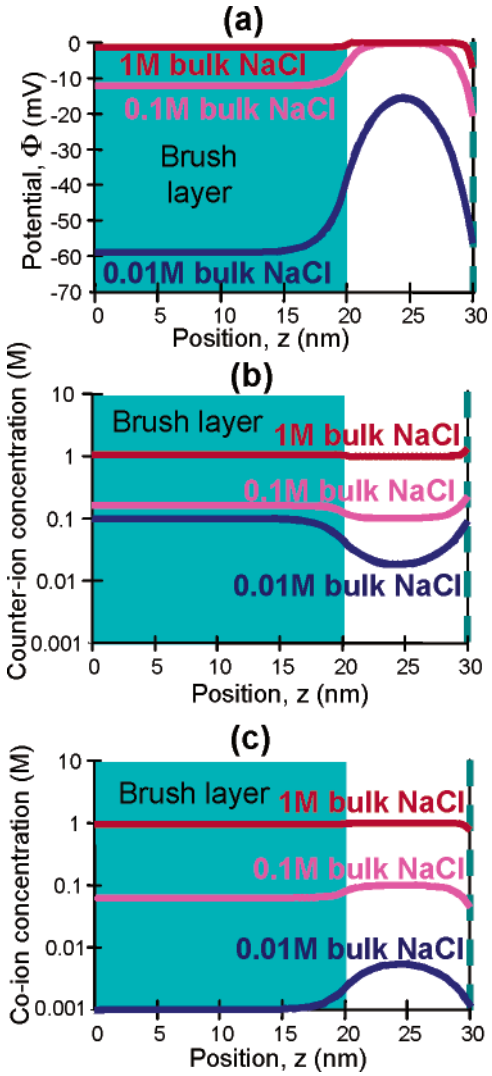

Figure 5. (a) Potential, Φ (mV), and (b) counterion and (c) co-ion concentrations for the volume charge model (Figure 1b) as a function of position, z (nm) for $h = 20$ nm; $D = 30$ nm; $C_0 = 0.01$ M, 0.1 M, and 1.0 M; $\rho_{volume} = -9.44 \times 10^6$ C/m^3 (0.0978 M); and $\sigma_1 = -0.015$ C/m^2. The blue shaded region on the left-hand side of the plot indicates the volume charge region, and the blue dashed line on the right-hand side of the plot indicates the flat surface charge.

in the bath because of the uniform, negative fixed charge density of the brush. The potential then increases to zero over a transition zone of approximately $3-5\ \kappa^{-1}$ at the brush−bath interface, is uniform within the bath, and then transitions to a negative value at the right-hand negatively charged surface, consistent with the fixed surface charge boundary condition there. As D decreases to be within a few κ^{-1} of h (i.e., $D < 25$ nm), the potentials due to the negative volume and surface charges interact strongly, and the net resulting potential is always negative (below the zero reference state). For $D < h$, the potential is uniform within the uniformly compressed brush region up to $3-5\ \kappa^{-1}$ from the surface and is increasingly negative as further compression (i.e., decreases in D) increases the negative volume charge density. The potential then transitions to a more negative value within a few Debye lengths of the surface charge σ_1. Noting that $C_0 = 0.1$ M is approximately equal to (ρ_{volume}/F), the counter- and co-ion concentrations within the brush layer (Figure 4b), calculated from the potential using eq 11, are never equal to $C_0 = 0.1$ M. In this region, the fixed volume charge density of the brush causes an increase in counterion (c_+) concentration and a decrease in co-ion (c_-) concentration, which is consistent with the macroscopic Donnan equilibrium ion partitioning that would be expected within the bulk of a uniform volume charge density in equilibrium with an electrolyte bath.[33,34]

Figure 4 highlights the effect of separation distance D on the potential and ion concentration profiles at $C_0 = 0.1$ M. In contrast, Figure 5 shows the effect of varying C_0 on Φ, c_-, and c_+, plotted as a function of position z between and normal to the surfaces for $D = 30$ nm. When ($|\rho_{volume}/F| \ll C_0$), for example, the case of $C_0 = 1.0$ M in Figure 5, the fixed charge groups in the brush are effectively screened by the abundant counterion concentration. Therefore, Φ in the brush layer is nearly equal to the zero bath reference potential, and the counter and co-ion concentrations in the brush are nearly equal to $C_0 = 1$ M. In this case, ρ_{volume} has a negligible effect on ion partitioning. In the opposite limit, when $|\rho_{volume}/F| \gg C_0$ (e.g., 0.01 M when the volume charge density in the brush layer is much greater than the bath NaCl concentration), Φ is substantially more negative in the negatively charged brush layer (Figure 5a), the counterion (Na^+) concentration

(33) Donnan, F. G. *Z. Electrochem.* **1911**, *17*, 572.
(34) Helfferich, F. *Ion Exchange*; McGraw-Hill: New York, 1962.

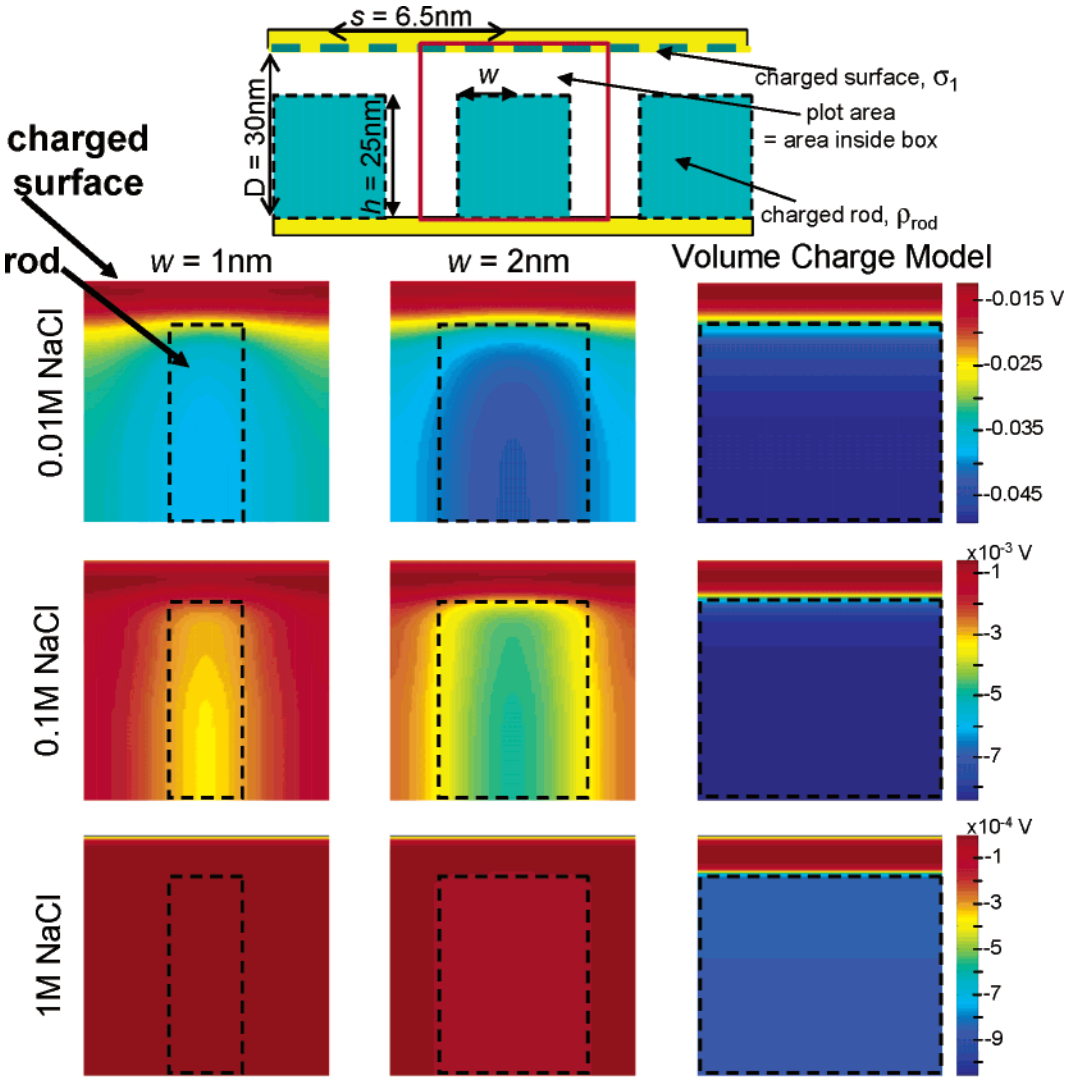

Figure 6. 2D potential distribution maps, Φ (mV), through the center of the rod for the charged rod model with two planar surfaces at $D = 30$ nm and $C_0 = 0.01$ M, 0.1 M, and 1.0 M NaCl, for $h = 25$ nm and $w = 1$, 2, and >3.67 nm (equivalent to volume charge model), at $s = 6.5$ nm and $\sigma_1 = -0.015$ C/m^2; the total fixed charge of the rod was constant, $Q = -8.00 \times 10^{-18}$ C.

is approximately equal to $|\rho_{volume}/F|$ (0.1 M, Figure 5b), and the co-ions are largely excluded from the brush, consistent with Donnan exclusion of co-ions[33,34] (Figure 5c, $[Cl^-] \approx 0.001$ M $\approx (|\rho_{volume}/F|^2/[Na^+])$. While the counterion concentration is much higher within the brush than in the bath, long-range electrostatic forces beyond the brush (between the brush and tip) will still exist as long as there is some degree of interaction (overlap) between the tails of the potential profile between tip and brush. The potential profile for 0.01 M bath NaCl (Figure 5a) shows that there is a significant interaction overlap even at $D = 30$ nm (i.e., the potential never decays to the zero reference value between $z = 20$ and $z = 30$ nm), which results in a long-range repulsive force.

Charged Rod Model. The potential above, between, and within the cylindrical rods of finite height having fixed uniform volume charge density is shown in two-dimensional cross section in Figure 6 for varying rod radii, w, in the range 1−3.67 nm and varying bath NaCl concentrations in the range 0.01−1 M. All other parameters representing the polyelectrolyte brush molecules and upper surface charge density are kept constant ($h = 25$ nm, total rod charge $Q = -8.00 \times 10^{-18}$ C, and $\sigma_1 = -0.015$ C/m^2). The variation of the potential profile for these conditions demonstrates how the nonuniform distribution of charge in the brush layer may affect both intra- and inter-rod electrostatic interactions. At a rod width of 1 nm (Figure 6), κ^{-1} (1 nm at 0.1 M NaCl) is smaller than the spacing between the edges of two adjacent rods (5.5 nm). Therefore, the potential distributions of two such adjacent rods will not significantly overlap (i.e., the potential between rods approaches the zero reference potential) and there will be little electrostatic repulsion interaction between rods. In contrast, at rod radii of 2−3 nm (0.1 M NaCl), or at 0.01 M NaCl even for thinner rod widths, there is significant interaction of the potential tails, and a significant repulsion force can be expected. At a rod radius greater than 3.67 nm, which is the limit of the volume charge model, the magnitude of the potential is larger everywhere and is uniform. However, the volume charge density is smaller and, therefore, the total force may be equal to or less than that predicted using thinner rods (see Figure 7). Thus, the various ionic strengths and rod radii in Figure 6 exhibit a range of force interactions that will be compared with the predictions of the surface and volume charge models below.

Comparison of Model Predictions of Electrostatic Force between Surfaces. From eqs 12 and 13 above, the potential profile can be used to calculate the electrostatic repulsion force between the surfaces for each of the three models of Figure 1. Model predictions are compared with each other in Figure 7. A noticeable discontinuity in

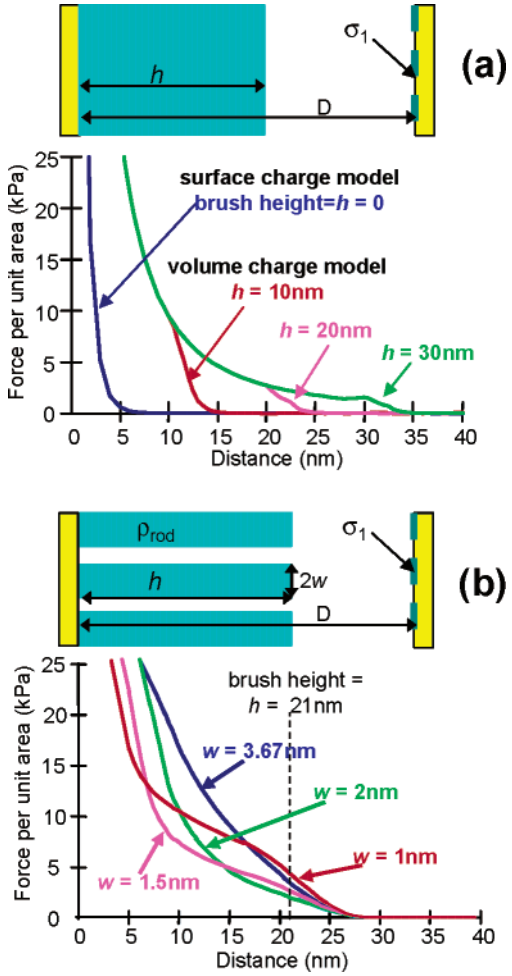

Figure 7. Simulation results of force per unit area (kPa) versus distance (nm) for two planar surfaces showing the effect of varying model parameters at $C_0 = 0.1$ M: (a) effect of varying h at constant $w = 3.67$ nm (volume charge model); (b) effect of varying w at constant $h = 21$ nm.

the slope of the force versus distance curves occurs when the charged tip encounters the top of the brush volume charge (Figure 7a). This is an intrinsic property of the volume charge model and was described previously by Ohshima.[12] For the parallel plate geometry of the volume charge model (Figure 7a), the force at any separation distance smaller than h is independent of h since model geometry and fixed charge density, ρ'_{volume}, are independent of h in this regime ($\rho'_{volume} = (\rho_{volume}h)/D = \sigma_{GAG}/D$). While all other parameters are kept constant, an increase in the initial brush height, h, will always increase the electrostatic force at separation distances greater than h (Figure 7a) since, as the brush height increases, fixed charges from the volume will be closer to the charged tip. Not surprisingly, the flat surface charge model (a volume charge in the limit $h \rightarrow 0$) will always predict a smaller electrostatic force than volume or rod models that account in some way for the height of the polyelectrolyte brush (Figure 7).

The discontinuity in the force versus distance curve of Figure 7a is much less apparent in the rod model at $D = h$ (Figure 7b) but does occur for smaller values of D when initially thin rods are forced to expand laterally by compression. When keeping the brush height constant, increasing the rod width changes the shape of the force curve (Figure 7b). As shown in Figure 6, increases in rod width will increase inter-rod electrostatic interactions; however, intra-rod interactions will decrease because the volume charge density decreases with increasing rod volume. In contrast, if the rod width is small, the force due to intra-rod repulsion will be high because the charge density inside the rod is very high, but inter-rod repulsion will be small since the edges of the rods are further apart.

Comparison of Model Predictions of Electrostatic Force to GAG Repulsive Force Data. To compare model force predictions to experimental data, the planar model geometry (Figure 1a−c) was converted to a hemispherical tip geometry (Figure 1d−f, see Appendix B). The best-fit model parameters are summarized in Table 2, and the surface charge model and best-fit curves for the volume and rod models are compared to data at different ionic strengths in Figure 8. All three models predict a decrease in repulsive force with increasing ionic strength. As expected and previously discussed,[6] the flat surface charge model greatly underestimates the force. While the rod and volume charge models both predict a transition in the force versus distance curve at the top of the brush, a sharp transition was not observed in the data, although it has been reported[26] to varying degrees with other polyelectrolyte systems. This may be due to the relatively low grafting density of GAGs (0.024 chains/nm^2) compared to other systems in the literature (e.g., 0.13−0.41 chains/nm^2 [26]).

The brush height can be estimated from the experimental data (Figure 8), since the electrostatic force begins at $D \sim 5\ \kappa^{-1}$ from the top of the brush. At a bath NaCl concentration of 0.01 M, κ^{-1} is ~3 nm. Therefore, since the measured experimental force starts at a tip−substrate separation distance of ~40 nm, the brush height should be ~25 nm. Similarly, $\kappa^{-1} \sim 1$ nm at 0.1 M NaCl, and the measured force begins at ~30 nm, so the brush height at 0.1 M is also expected to be ~25 nm. At 1.0 M NaCl, $\kappa^{-1} \sim 0.3$ nm, and the measured force begins to increase at ~20 nm; therefore, the estimated brush height at that ionic strength is ~19 nm.

At 0.1 and 0.01 M NaCl, the volume charge model predicts a much closer fit to the data than the surface charge model. However, the best-fit value of h (the one adjustable parameter) is 14 nm at 0.1 M and 18 nm at 0.01 M (Table 2), which is ~2-fold smaller than the known extended GAG length. These values do not appear to be well predicted by the volume charge model since they are small compared to the value of the brush height estimated from the force curves. However, this result may be expected since the GAG chains are about 6.5 nm apart and the volume charge model assumes a uniform volume charge density. In distinct contrast, the rod model predicted a much better agreement with the force data for reasonable best-fit values of h and w at both 0.01 and 0.1 M NaCl (Figure 8a,b). The values for h are consistent with the estimate from inspection of the force curve. This best-fit height suggests that the molecules are neither fully extended nor fully collapsed onto the surface. The best-fit w is about 4 times larger than the known radius of the CS-GAG molecule.[35] However, the rods in the model represent the time-average space occupied by the molecule and not the molecule itself and there are no previous measurements of this parameter for CS-GAG molecules in a brush. The best-fit value of w suggests that the CS-GAG molecules are not rigid but are undergoing random thermal motion within their tethered constraint.

The models presented here include only electrostatic (and not steric) forces. When electrostatic forces dominate (i.e., for IS ≤ 0.1 M), the model is able to predict values

(35) Maroudas, A. In *Adult Articular Cartilage*; Freeman, M. A. R., Ed.; Pitman Medical: Kent, U.K., 1979; pp 215−290.

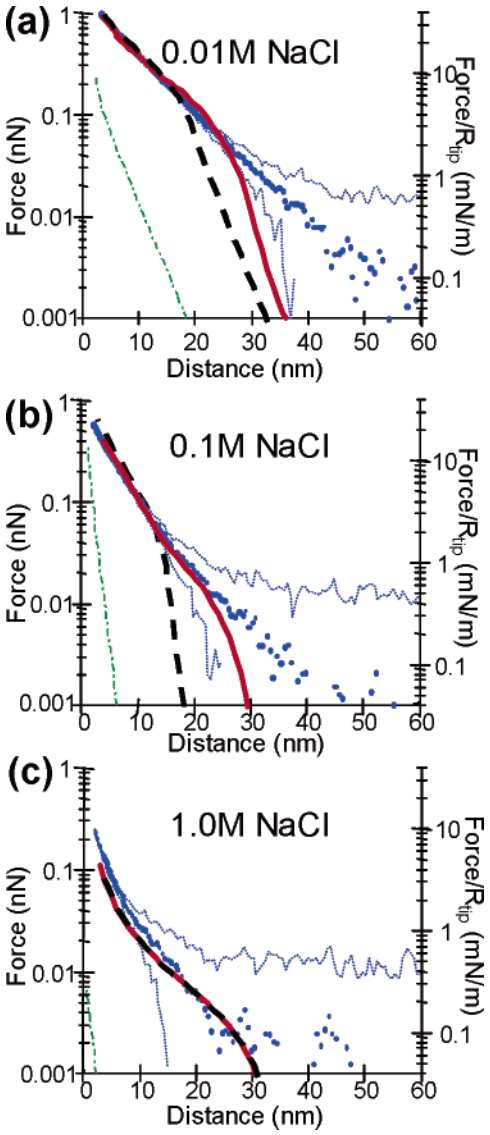

Figure 8. Comparison of best-fit charged rod (solid red line), volume (dashed black line), and surface charge models (dot−dash green line) for a charged hemispherical probe tip versus a planar surface to high-resolution force spectroscopy data (blue dots, standard deviation = dotted blue line) obtained on approach using a sulfate-functionalized probe tip versus an end-grafted CS-GAG polymer brush. (a) $C_0 = 0.01$ M NaCl. Rod model parameters: $h = 25$ nm, $w = 2$ nm. Volume model: $h = 18$ nm. Surface model: no fitting parameters. (b) $C_0 = 0.1$ M NaCl. Rod model parameters: $h = 25$ nm, $w = 2$ nm. Volume model: $h = 14$ nm. Surface model: no fitting parameters. (c) $C_0 = 1$ M NaCl. Rod model parameters: $h = 32$ nm, $w = 3.67$ nm (rod model = volume model). Volume model: $h = 32$ nm. Surface model: no fitting parameters. The fixed parameters were $s = 6.5$ nm, $Q = -8.00 \times 10^{-18}$ C, $\sigma_1 = -0.015$ C/m^2, and $R_{tip} = 25$ nm.

for the brush height that are not significantly affected by the presence of steric forces, consistent with the assumptions of the models. However, at 1 M salt concentration ($\kappa^{-1} \sim 0.3$ nm), electrostatic forces are on the order of steric interactions at tip−substrate separation distances smaller than the brush height. Therefore, by fitting the brush height of any purely electrostatic model to the total measured force in this high-salt regime, the brush height is overestimated in order to compensate.

Extensions of the Charged Rod Model to Polyelectrolyte Brush−Brush Interactions. Experiments are currently underway to measure the force between two

Table 2. Model Predictions of Electrostatic Forces and Comparison to Experimental Data: Best-Fit Values of Model Parameters at Different Bath Ionic Strengths

	volume charge model	rod charge model	
	volume height, h (nm)	rod height, h (nm)	rod radius, w (nm)
0.01 M NaCl	18	25	2
0.1 M NaCl	14	25	2
1.0 M NaCl	32	32	3.67

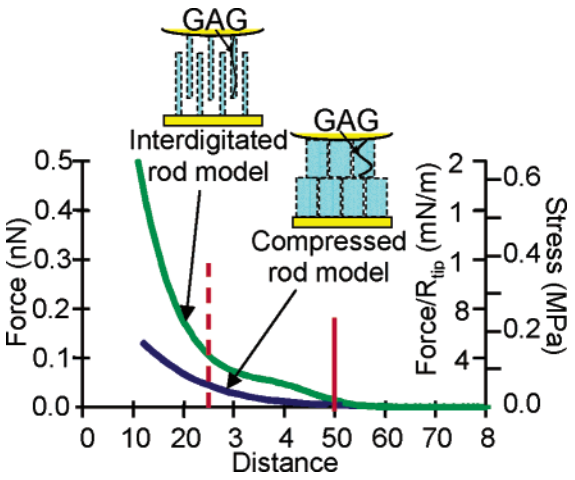

Figure 9. Comparison of two different molecular mechanisms of deformation using the charged rod model for the electrostatic repulsion force between two opposing polyelectrolyte brushes, one on a planar surface and the other on a hemispherical probe tip; force (nN), force/R_{tip} (mN/m), and stress (MPa) versus distance (nm) are plotted for $C_0 = 0.1$ M, $h = 25$ nm, $w = 2$ nm, and $R_{tip} = 25$ nm. In one model the rods interdigitate, and in the other model the two brushes exclude and compress each other. The vertical red line at 50 nm indicates the distance at which the two brushes just become in physical contact, and the vertical red dashed line at 25 nm indicates the height of one brush.

adjacent GAG brush layers,[36] which is more representative of native cartilage. Figure 9 shows two different extensions of the rod model to describe such brush−brush electrostatic interactions, one in which the brush layers exclude each other and the other in which the brushes can interdigitate. There are significant differences in the predicted force between these two models, even though the total brush fixed charge is constrained to be the same in each. The compressed, noninterdigitating model predicts a force that is essentially a doubling of the force arising from a single brush. In contrast, the interdigitating model inherently incorporates more brush−brush repulsive forces since the rods from the two opposing brushes are interspersed three-dimensionally and therefore exhibit increased electrostatic repulsive interactions. These differences in brush−brush electrostatic interactions can only be incorporated into models that include aspects of molecular-level structure (e.g., the volume and rod models). Currently, no theoretical model exists to describe the steric interactions between interdigitating surfaces of end-grafted rods. It is not currently known whether GAG molecules interdigitate within native cartilage tissue. Hopefully, a combination of HRFS measurements, atomic force microscopy (AFM) visualization, and theoretical modeling can help to determine how these molecules are arranged in tissues.

(36) Seog, J.; Frank, E.; Dean, D.; Wong-Palms, S.; Plaas, A. H. K.; Grodzinsky, A.; Ortiz, C. In *Transactions of the 48th Orthopaedic Research Society Meeting*; Orthopaedic Research Society: Dallas, 2002; Vol. 27.

Relevance to Modeling Native Cartilage under Physiological Conditions. *Steric Forces.* In native cartilage (IS ∼ 0.15 M, synovial fluid pH ∼ 7.4, intracartilage pH ∼ 6.5−7), aggrecan molecules are precompressed to occupy only ∼20% of the volume taken up under dilute solution conditions. Further compaction of aggrecan is caused by compressive strains as high as 15−30% that may result from static joint loading under normal physiological conditions. As a result, the average separation distance between GAG chains in the tissue is ∼2−5 nm[3] and, hence, values of D in our HRFS experiments in the range of <10 nm are most relevant to modeling native cartilage. Given this dense packing, macromolecular steric repulsive forces between GAGs might also contribute to the total net osmotic swelling stress and compressive stiffness of cartilage. Steric forces may include configurational,[37] mixing, and translational entropies, as well as enthalpic disruption of supramolecular structure (e.g., due to GAG−water hydrogen bonding[38]). The magnitude and range of steric forces depend on the conformation of the constituent GAG chains within tissue which is unknown (i.e., rigid rod versus random coil), their equilibrium position in space (i.e., in HRFS experiments, standing up versus lying down), and their molecular configuration during deformation (i.e., interdigitation versus compression).

In relating the present model to cartilage, additivity of steric and electrostatic forces may be assumed to a first approximation,[37,39] knowing that both of these components are dependent on solution environmental conditions (IS, pH) and, hence, interrelated to each other. Kovach[39] recently estimated the contributions of the configurational and mixing entropies of aggrecan-associated CS-GAGs to the equilibrium elasticity of cartilage and to the elasticity of solutions of aggrecan. These results were compared to measurements of the corresponding macroscopic properties of aggrecan and cartilage. Kovach demonstrated that in 1.5 M salt, the conformational contribution to the swelling pressure of CS-GAGs was ∼30%, but at physiologic IS, the contribution was only ∼10%. He thus concluded that the electrostatic repulsive contribution was the predominant factor in determining the equilibrium swelling pressure of cartilage under physiological conditions. Theoretical work on the translational entropy component of the steric interaction of an incoming particle with surface-grafted rods[37] suggests that the repulsive force has a nonlinear form with decreasing D and becomes significant for $D <$ brush height. To model this component of the force in HRFS experiments rigorously, one would need an independent experimental measurement of the brush height, for example, by ellipsometry or neutron reflectivity. Currently, no theoretical model exists to describe the interaction between end-grafted interdigitating rods.

Hard-Wall Substrate in HRFS. In relating the configurations of Figure 1 to the modeling of cartilage, there is no equivalent in the tissue of the "hard-wall" planar substrate. Hence, even though this model may be appropriate for HRFS, further extensions are needed for application to the deformation of native cartilage. However, changes in force due to changes in D (i.e., the derivative of the force versus D curve) may be a good predictor of the electrostatic contribution to the cartilage elastic modulus; ongoing studies are aimed at testing this hypothesis.

Divalent Ions. In addition, cartilage interstitial fluid in vivo contains a small proportion of the divalent ion, calcium (<5%[35]), which can easily be incorporated into the model via eq 8 and will only cause a small decrease in the predicted electrostatic force (∼1%) using the PB formulation. While the presence of multivalent counterions has been reported to induce attractive interactions between like-charged polyelectrolyte chains such as DNA under specialized conditions,[40] this has not been observed for cartilage under physiological buffer conditions.[41]

Charge Sequence Along GAG Backbone. GAGs are known to have charge heterogeneity in type of functional group and local charge density[42] that may affect both steric and electrostatic interactions at the atomic level. While this is not taken into account directly in our models, molecular dynamics models at the atomic level may be able to determine the importance of this phenomenon.

Conclusions

We have compared three models for the electrostatic interaction forces within a polyelectrolyte brush layer. The rod model has been shown to be a feasible alternative to the simpler models previously discussed in the literature. Although the total polyelectrolyte charge was the same in all three models, both the rod and volume charge models, which accounted for the height of the brush, predicted much higher forces than the surface charge model at any given separation distance. The comparison between measured and theoretically predicted forces in Figure 8 shows that the rod model gives better agreement with the force data over the widest range of separation distance D and for reasonable best-fit values of the brush height and rod radius. Changes in the rod radius led to changes in the shape of the predicted force profile. Therefore, in the framework of the PB theory, it appears that molecular-level changes in the charge distribution inside polyelectrolyte brush layers as manifested in the rod model can significantly change the magnitude and the shape of the resulting force profile. Although the rod model is more general, it is also significantly more computationally intensive than the other two models. In certain experimental regimes, the volume charge model may be sufficient (e.g., when the polyelectrolyte molecules are less than κ^{-1} apart). Future work includes comparing the predictions of these models to more complex experimental systems (such as the ongoing GAG brush−brush interaction experiments described above) and to the predictions of atomic-level models of GAGs and GAG−GAG interactions.[43]

Acknowledgment. This research was supported by National Institutes of Health Grant AR45779, the DuPont−MIT Alliance, and a Whitaker Foundation graduate fellowship (D.D.).

Appendix A: Charge Titration at Surfaces

As stated in the text, we used constant charge rather than constant potential boundary conditions on the surface of the tip and the substrate. In general, the pH at a charged

(37) Miller, I.; Williams, D. *Phys. Rev. E*: *Stat. Phys., Plasmas, Fluids, Relat. Interdiscip. Top.* **2000**, *61*, R4706−R4709.
(38) Oesterhelt, F.; Rief, M.; Gaub, H. E. *New J. Phys.* **1999**, *1*, 6.1−6.11.
(39) Kovach, I. S. *Biophys. Chem.* **1996**, *59*, 61−73.
(40) Ha, B.-Y.; Liu, A. J. *Phys. Rev. E* **1999**, *60*, 803−813.
(41) Grodzinsky, A. J.; Roth, V.; Myers, E.; Grossman, W. D.; Mow, V. C. *J. Biomech. Eng.* **1981**, *103*, 221−231.
(42) Plaas, A. H.; West, L. A.; Wong-Palms, S.; Nelson, F. R. *J. Biol. Chem.* **1998**, *273*, 12642−12649.
(43) Bathe, M.; Rutledge, G. C.; Grodzinsky, A. J.; Tidor, B. In *Computational Fluid and Solid Mechanics*; Bathe, K. J., Ed.; Elsevier Science Ltd.: 2003.

surface will differ from the pH of the adjacent fluid bath since the concentration of H^+ and all other mobile ions will vary with the electrical potential away from the surface.[44] The ionization state of the surface charge groups and the surface pH will depend on bath pH, bath ionic strength, and the pK_a's of the ionizable charge groups. A lower bound estimate of the surface pH was calculated using the linearized PB equation, and from this, we calculated the self-consistent upper bound for the concentration of the protonated form of the charged groups on the surface.

The local ion concentration depends on the potential, Φ (eq 6). For small enough Φ, (i.e., $F\Phi/RT \ll 1$), linearization of the PB equation gives

$$\nabla^2\Phi \approx \frac{2FC_0}{\epsilon_w}\left(\frac{F\Phi}{RT}\right) = \kappa^2\Phi \qquad \text{(A.1)}$$

Similarly, linearization of the local ion concentrations (eq 6) gives an expression for the H^+ concentration:

$$c_{H^+}(z=0) = \bar{c}_{H^+}\exp\left[-\frac{F\Phi(z=0)}{RT}\right] \approx \bar{c}_{H^+}\left(1 - \frac{F\Phi(z=0)}{RT}\right) \qquad \text{(A.2)}$$

where $c_{H^+}(z=0)$ is the H^+ concentration at the surface at $z=0$, $\bar{c}_{H^+}$ is the known (measured) bulk H^+ concentration (given from the bulk pH of the solution), and $\Phi(z=0)$ is the surface potential. The linear approximation will give a tight lower bound even if the potential is not small enough since $\exp(-\Phi F/RT) > 1 - \Phi F/RT$ is always true. Therefore, since the local pH is

$$\mathrm{pH}(z=0) = -\log(c_{H^+}(z=0)) \qquad \text{(A.3)}$$

the pH calculated from the linear approximation of the PB (eq A.1) equation will always be lower than the pH calculated from solution of the full nonlinear equation. Given charged parallel plates of infinite extent (Figure 1a), solution of the linearized PB equation for the potential, $\Phi(z)$, between the plates gives

$$\Phi(z) = \frac{\sigma_1\cosh(\kappa(z-D)) + \sigma_2\cosh(\kappa z)}{(\kappa\epsilon_w)\sinh(\kappa D)} \qquad \text{(A.4)}$$

where D is the separation distance between the two plates, σ_1 is the surface charge density of the plate at $z=0$, and σ_2 is the surface charge density of the plate at $z=D$. We first consider the case of equally charged surfaces, $\sigma_1 = \sigma_2 = \sigma$. We also assume that the ionization processes can be described by a reversible bimolecular dissociation reaction leading to the form of a Langmuir charging isotherm in which the surface charge density, σ, will vary with the pH of the surface:[45]

$$\sigma = \frac{K}{K + c_{H^+}(z=0)}\sigma_{max} \qquad \text{(A.5)}$$

where K is the dissociation constant of the charge groups on the surface ($K = 10^{-pK}$) and σ_{max} is the maximum charge density if all the groups on the surface were charged. From eqs A.2 and A.4, we can solve for $c_{H^+}(z=0)$:

$$c_{H^+}(z=0) = \frac{1}{2}\left(\bar{c}_{H^+} - K + \sqrt{(\bar{c}_{H^+}+K)^2 - 2\frac{\bar{c}_{H^+}K\sigma_{max}\kappa(\cosh(\kappa D)+1)}{FC_0\sinh(\kappa D)}}\right) \qquad \text{(A.6)}$$

In the limit $\kappa D \gg 1$, eq A.6 reduces to the H^+ concentration at a single charged plate:

$$c_{H^+}(z=0) = \frac{1}{2}\left(\bar{c}_{H^+} - K + \sqrt{(\bar{c}_{H^+}+K)^2 - 2\frac{\bar{c}_{H^+}K\sigma_{max}\kappa}{FC_0}}\right) \qquad \text{(A.7)}$$

In the limit when $\kappa D \ll 1$, $c_{H^+}(z=0)$ becomes very large and tends to infinity:

$$c_{H^+}(z=0) = \frac{1}{2}\left(\bar{c}_{H^+} - K + \sqrt{(\bar{c}_{H^+}+K)^2 - \frac{\bar{c}_{H^+}K\sigma_{max}(4+(\kappa D)^2)}{FC_0D}}\right) \qquad \text{(A.8)}$$

This latter nonphysical limit is a result of the PB assumption that ions take up no volume.

From eq A.8, the surface pH will be lowest when the ionic strength is low and when κD is small. Therefore, to determine whether constant charge boundary conditions were appropriate, we calculated the percentage of charged groups on the surface that would be neutralized (protonated) at $D = \kappa^{-1}$ versus $D \to \infty$ at 0.01−1.0 M NaCl, pH 5.5. The effective surface charge density, σ, is plotted as a function of normalized separation distance in Figure 10 for the case where all charges are assumed to be on the surface and are either carboxyl or sulfate groups alone, and assuming a maximum charge density (σ_{max}) of −0.1 C/m^2. Values of σ for the case of 0.01 M NaCl bath concentration are tabulated in Table 3.

As shown in Table 3 and Figure 10, there is very little change in the surface charge density if all the charge groups are due to sulfate groups and, for such a case, the assumption of constant charge on the tip seems appropriate. GAG molecules contain carboxyl as well as sulfate groups. If all the charge due to carboxyl groups in the GAG molecules were placed on the surface of the substrate, there would be a ∼15% change in the effective surface charge density as the tip and the substrate are brought to a separation of 3 nm at 0.01 M NaCl; at 0.1 M NaCl, there would only be a 5.8% change in the surface charge density as the tip and substrate are brought to a separation of 1 nm.

However, the carboxyl and sulfate groups in our experiment are on GAG chains and, as such, are not directly on the surface of the substrate. In three dimensions, the GAG charge groups could be modeled as a volume charge density above a neutral substrate as in Figure 1b. The titration of charge groups within a volume charge density can be described as follows:[45]

$$\rho_{volume} = \rho_{max}\frac{K}{K + c_{H^+}(z)} = \frac{\sigma_{max}^{brush}}{h}\left(\frac{K}{K + c_{H^+}(z)}\right) \qquad \text{(A.9)}$$

where ρ_{volume} is the volume charge density of the brush, h is the height of the brush, $\rho_{max} = \sigma_{max}^{brush}/h$ is the maximum charge density when all the groups in the brush are ionized, and $c_{H^+}(z)$ is the local H^+ concentration inside the brush. This is a two-region problem, and therefore the linear PB equation (eq A.1) has an added charge term

(44) Ninham, B. W.; Parsegian, V. A. *J. Theor. Biol.* **1971**, *31*, 405−428.

(45) Tanford, C. *Physical chemistry of macromolecules*; John Wiley & Sons: New York, 1961.

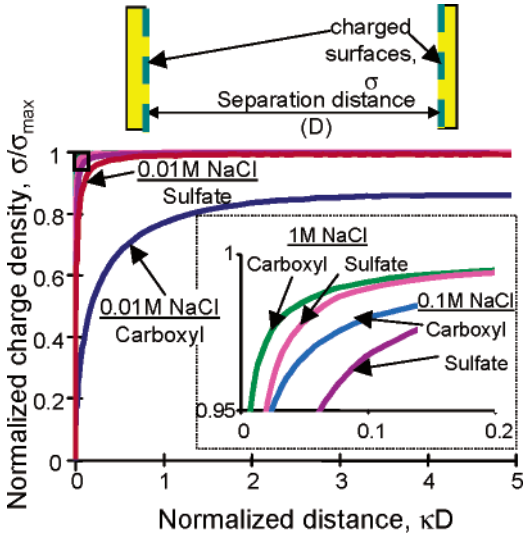

Figure 10. Theoretical calculation for normalized surface charge as a function of separation distance using the surface charge model between two planar surfaces at pH 5.5 and different bath NaCl concentrations assuming all the surface charges are due to sulfate groups with p$K_a = 2$ or assuming all the surface charges are due to carboxyl groups with p$K_a = 3.5$. The inset is an expansion of the curves in the top left corner rectangle.

Table 3. Calculated Surface Charge Density if Titration Is Taken into Account Assuming a Bath NaCl Concentration of 0.01 M with No pH Buffers in the Bath, a Maximum Surface Charge Density of −0.1 C/m², and That All the Charges Are Either All Carboxyl or All Sulfate Groups Alone

charged group type	$D = \kappa^{-1}$	$D \rightarrow \infty$
carboxyl groups (p$K_a = 3.5$) (ref 47)	−0.0750 C/m²	−0.0860 C/m²
sulfate groups (p$K_a = 2$) (ref 48)	−0.0987 C/m²	−0.0995 C/m²

inside the brush:

$$\nabla^2\Phi \approx \kappa^2\Phi - \frac{\rho_{volume}}{\epsilon_w} \qquad \text{for } 0 < z < h \quad \text{(A.10)}$$

This equation can be solved analytically subject to the following boundary conditions:

$$\frac{\partial}{\partial z}\Phi|_{z=0} = 0$$

$$\frac{\partial}{\partial z}\Phi|_{z=h_+} = \frac{\partial}{\partial z}\Phi|_{z=h_-}$$

$$\Phi|_{z=h_+} = \Phi|_{z=h_-}$$

$$\frac{\partial}{\partial z}\Phi|_{z=D} = \frac{\sigma_{tip}}{\epsilon_w} \qquad \text{(A.11)}$$

For brush height larger than κ^{-1}, the potential inside the brush (i.e., $0 < z < h$) is

$$\Phi = -\frac{\sigma_{brush}}{2\epsilon_w h}z^2 + \frac{\sigma_{brush}e^{-\kappa h}}{h}\left(\frac{h^2}{2\epsilon_w} + \frac{h}{\kappa\epsilon_w}\right)\cosh(\kappa h) \qquad \text{when } D \gg h \quad \text{(A.12)}$$

$$\Phi = -\frac{\sigma_{brush}}{2\epsilon_w D}z^2 + \frac{\sigma_{tip}}{\kappa\epsilon_w}\left(\frac{\cosh(\kappa z)}{\sinh(\kappa D)}\right) \qquad \text{when } D = \kappa^{-1}$$

where $\sigma_{brush}/h = \rho_{volume}$. Using this brush potential, one can first calculate the H^+ inside the brush and then the total charge in the brush as a function of separation distance, D. When setting $\sigma_{tip} = -0.1$ C/m², $h = 10$ nm, and $\sigma_{max}^{brush} = -0.1$ C/m² and assuming all the charge in the brush is due to carboxyl groups, then at 0.01 M bath NaCl, the total charge in the brush changes by at most 7% when the tip and substrate are brought to within one Debye length of each other (see Table 4).

Table 4. Average Value of Volume Charge Density if Titration Is Taken into Account Assuming a Bulk NaCl Concentration of 0.01 M, a Maximum Volume Charge Density of -10×10^6 C/m³, and That All the Charges Are Due to Either Carboxyl or Sulfate Groups

charged group type	$D = \kappa^{-1}$	$D \rightarrow \infty$
carboxyl groups (p$K_a = 3.5$)	-9.1×10^6 C/m³ (0.094 M)	-9.8×10^6 C/m² (0.10 M)
sulfate groups (p$K_a = 2$)	-10×10^6 C/m² (0.10 M)	-10×10^6 C/m² (0.10 M)

This value is still a tight upper bound on the change in charge as a function of distance since we used the upper bound on the tip and brush charges and the lower bound on the brush height. Therefore, it seems reasonable to assume that the charge is constant as a function of separation distance and constant charge conditions are appropriate. Of course, if the bulk pH were much lower or if the charge groups had higher pK_a, one would need to include titration into the models discussed here as described. The boundary conditions and volume charge densities would then be functions of the potential. For example, the boundary condition on the substrate could change to $(\partial/\partial z)\Phi = -\sigma/\epsilon_w$ at $z = 0$ where

$$\sigma = \sigma_{max}\frac{K}{K + \bar{c}_{H^+}\exp\left[-\frac{F\Phi(z=0)}{RT}\right]}$$

and it is still possible to solve the nonlinear PB equation with these more complicated expressions for the charge densities using the same numerical techniques used here.

Appendix B: Hemispherical Tip Approximation

All the models associated with Figure 1a−c were solved numerically for a plane parallel geometry. However, in the experiments, the probe tip is a blunted pyramid (Figure 2b) that can be modeled as a hemisphere, since the distances probed are on the order of the radius of curvature. Therefore, the calculated forces between planar surfaces were converted to approximations of the force between a flat substrate and a hemispherical tip. The method, based on the original formulation of Derjaguin[32] and sometimes known as surface element integration (SEI),[16] is the numerical version of the integral of a uniform normal stress or pressure over the surface of the hemisphere tip. This method will give the appropriate total force only if the stress (force per unit area) is everywhere normal to the surface. For the case of electrostatic forces, this requirement is automatically met if the surface is an equipotential (i.e., the case of a constant potential boundary condition[16]), since the electric field and therefore the electrical stress are everywhere normal to an equipotential surface. However, when a curved probe tip or a noninfinite

(46) Israelachvili, J. N. *Intermolecular and Surface Forces*, 2nd ed.; Academic Press: London, 1992.
(47) Freeman, W. D. S. C.; Maroudas, A. *Ann. Rheum. Dis.* (*Suppl.*) **1975**, *34*, 44−45.
(48) Kuettner, K.; Lindenbaum, A. *Biochim. Biophys. Acta* **1965**, *101*, 223−225.

planar surface (e.g., the substrate under the brush) has a constant charge density, that surface is no longer an equipotential and the **E**-field and electrical stress will not be everywhere normal to the tip and substrate surfaces. This approximation method will then underestimate the total force, since tangential components of the stress are not taken into account. Therefore, this method can only be used to estimate the force between a constant charge hemispherical tip and a substrate when the radius of the tip is much larger than κ^{-1}, since the tangential components of the stress will then be small. This method has advantages over the standard Derjaguin approximation[14,46] in which the force between a hemisphere and plane separated by distance D is approximated by calculating the force per unit area between two infinite planes separated by D and then multiplying by $2\pi R_{\text{hemisphere}}$. This latter Derjaguin approximation is only valid when $R_{\text{hemisphere}}$ is very large compared to D. Although this approximation is typically justified for the geometry of the surface force apparatus,[46] it is not justified with many AFM probe tip geometries such as ours using a probe tip radius of 25 nm. The SEI Derjaguin approximation is valid for any value of D as long as $R_{\text{hemisphere}}$ is larger than κ^{-1}. In addition, it can be used for geometries other than hemispherical, while the standard Derjaguin approximation is only valid for convex tip geometries.

Abbreviations

CS-GAG	chondroitin sulfate glycosaminoglycan
FDM	finite difference method
HRFS	high-resolution force spectroscopy
IS	ionic strength
MFP	molecular force probe
PB	Poisson−Boltzmann
RHS	right-hand side
SEI	surface element integration

Symbols

c_-	concentration of − ions
c_+	concentration of + ions
C_0	bath NaCl concentration
c_{H^+}	local concentration of H^+ ions
$\bar{c}_{H^+}$	bath concentration of H^+ ions
c_i	local concentration of ith ionic species
c_{io}	bath concentration of ith ionic species
D	separation distance
E	electric field
F	Faraday's constant
F_z	electrostatic force in the z-direction
h	brush height in model
H	magnetic field
K	dissociation constant
N	number of discretizations
Q	fixed charge of one polyelectrolyte molecule
q	charge
R	gas constant
$R_{\text{hemisphere}}$	radius of hemisphere tip in model
R_{tip}	radius of curvature of the probe tip
s	spacing between polyelectrolyte molecules in brush
T	temperature
w	radius of cylindrical volume of charge in model
W_e	electrostatic free energy
z	position
z_i	valence of ith ionic species
Φ	electrical potential
ϵ_w	dielectric permittivity of water
κ^{-1}	Debye length
ρ_{fix}	volume charge density due to fixed charge groups
ρ_{max}	maximum volume charge density when all groups are ionized
ρ_{mobile}	volume charge density due to mobile ions in solution
ρ_{rod}	effective volume charge density due to the time-average space taken up by polyelectrolyte molecule
ρ_{total}	total local volume charge density
ρ_{volume}	effective volume charge due to polyelectrolyte brush
σ_1	surface charge density on top planar surface
σ_2	surface charge density on bottom planar surface
σ_{GAG}	effective surface charge density due to GAG brush
σ_{max}	maximum surface charge density when all groups are ionized
σ_{tip}	surface charge density on probe tip

LA027001K